eJSE International

Special Issue: Electronic Journal of Structural Engineering 14(1) 2015

Damage and Seismic Performance Assessment of FRP-Retrofitted Multi-Storey RC Buildings

S. S. MAHINI

Discipline of Civil and Environmental Engineering, University of New England, NSW, Australia

Email: smahini@une.edu.au

ABSTRACT: Structures should be designed for a long in-service life at the lowest cost. Performance based design (PBD) can be used for damage and performance assessment of older FRP-retrofitted multi-storey RC moment resisting frames (MRFs). PBD can be performed using nonlinear pushover analysis according to current codes. In this paper, performance of an existing/older RC frame that has been retrofitted with steel-braced by other researchers is assessed in order to evaluate the ability of the FRP-web bonded system to upgrade the performance level and ductility of RC MRFs.

Initially, the flexural stiffness of FRP-retrofitted exterior and interior joints of each level of an existing RC ordinary moment resisting frame (OMRF) is determined using nonlinear finite element (FE) analysis. The stiffness obtained is then used in a mathematical model for pushover analysis of the FRP-retrofitted frame. The plain and the retrofitted frames (both steel-braced and FRP-retrofitted) are analysed using a nonlinear pushover analysis method. The seismic performances of the retrofitted frames are then compared with the plain frame. Finally, the global damage index of the frames at the performance point (and at the life safety (LS)) are determined from the capacity curves and discussed. This evaluation demonstrates that the damage degree of the frame is reduced after retrofitting particularly by FRP. In addition, the FRP-retrofitted frame has a lower damage index at the LS level.

Keywords**:** *Damage, Performance assessment, RC frame, Web-bonded FRP, Steel braced, Damage index.*

1 INTRODUCTION

Many existing RC structures may be vulnerable to failure because of structural weaknesses and low ductility. Common weaknesses in RC buildings are incomplete load paths, strength and stiffness discontinuities, weak column and strong beam, vertical, horizontal and mass irregularities and eccentricities. Insufficient shear reinforcement, inadequate confinement, and insufficient anchorage length of the beam-reinforcement bars can be characterised as low ductility detailing.

In recent years, the performance-based design method has been added to seismic design codes worldwide. In the newly-developed seismic design approach, nonlinear pushover analysis is important in identifying the damage patterns and ductility levels for assessing the structure's inelastic behaviour and for understanding the seismic failure modes of the structure for retrofitting purposes. Pushover analysis estimates the seismic displacement demand of the structure with an Equivalent Single Degree Of Freedom (ESDOF) system and allows monitoring of global and local deformations, yielding process and strength deterioration.

The use of steel braces has been popular for the retrofitting of RC frames as a shear resisting element in the seismic design of new buildings in order to increase the shear capacity of existing buildings (Hadigeh et al., 2014). In this regard, Maheri and Akbari (2003) examined steel-braced RC dual systems for improving the ductility level of the moment resisting frame. They indicated that when designed for a specific base shear, steel-braced RC dual systems possess much higher ductility levels than their equivalent unbraced MRFs.

In the last two decades, fibre-reinforced polymers (FRP) have also been utilised for this purpose. Parvin & Granata (2000) indicated that when joints of an RC frame were reinforced with FRP laminates, the moment capacity is increased by 37%. In addition, Mahini (2005) and Mahini and Ronagh (2010, and 2011) proposed a new method for the strengthening of exterior beam-column joints using web-bonded FRPs. They investigated the effectiveness of

web-bonded CFRP on the energy absorption capacity of 1/2.2 scale RC joints in order to evaluate the possibility of relocating the plastic hinge location away from the face of the column. Mahini (2005) concluded that the method was effective and practical. In another experimental study, Balsamo et al. (2005) evaluated the seismic behaviour of a full-scale RC frame repaired using CFRP laminates. They indicated that the repaired frame had a large displacement capacity without exhibiting any loss of strength and provided energy dissipation similar to that of the original frame.

Niroomandi et al. (2010) assessed the performance of a FRP retrofitted RC frame. The moment-rotation relationship of the RC joints retrofitted with web-bonded CFRP, as developed by Mahini (2005) and Mahini and Ronagh (2010), was obtained using ANSYS software. They showed that the performance level and the seismic behaviour factor of the FRP retrofitted RC frame was improved or even significantly enhanced in comparison with the original frame. Niroomandi et al. (2010), concentrated on the peak strength of the plain/retrofitted joints in their study. Hadigheh et al. (2014) obtained additional moment-rotation stiffness of the FRP-retrofitted joints using ABAQUS finite element software and proved that the superior performance of *weak beam-strong column* RC frames strengthened at the joints by FRP.

In terms of the damage evaluation, Haoxiang et al. (2013) presented a global damage index based on multiple linear force-deformation curves in pushover analysis in order to evaluate the integrated damage of RC structures. In their study, the damage-index was adjusted, considering the displacement and energy of structures, based on performance-based seismic design. An evaluation method was proposed by applying fuzzy set theory. It was concluded that, this method can be achieved based on pushover analysis, code spectrum, and the capacity spectrum method (Haoxiang et al., 2013). Naeim (2013), also implemented schemes to provide real-time performance and damage information for buildings and other types of structures. However, these methods have not been utilized for damage evaluation of FRP-retrofitted multi-storey RC buildings.

This paper assesses the performance of an existing plain RC MRF and also FRP-retrofitted and steel-braced frames. For this purpose, an eight storey RC building which was retrofitted by Maheri and Akbari (2003) using steel bracing systems was retrofitted with the CFRP web-bonded technique in order to assess and compare the seismic performance. The retrofitted joints stiffness in the form of moment–rotation relation was determined in detailed FE modelling of the composite joints and the results then utilised to carry out nonlinear pushover analysis of a selected full frame in order to evaluate its force–displacement capacity curve. The seismic performances of the FRP-retrofitted frames was then compared with the corresponding plain frame.

Finally, performances of retrofitted multi-storey RC frames were evaluated and a global damage index proposed. The global damage index for capacity curve of plain/retrofitted frames at the capacity (performance) point as well as life safety was obtained and the results compared with the research using performance based-design criteria.

2 FRP-RETROFITTING SCHEME

In this paper, repairing/retrofitting is undertaken using a new technique called web-bonded FRP system, by Mahini (2005). This method works by bonding FRP sheets of specific lengths to the sides of the RC beam's ends leading to the joints. Experimental studies showed that the FRP repairing/retrofitting system can restore/upgrade the integrity of the joint, keeping/upgrading its strength, stiffness and ductility, and shifting the plastic hinges from the column face toward the beam in such a way that the joint remains elastic. Figure 1 shows the failure mechanism of a scaled down beam-column joint (CSM0) before and after retrofitting (RPSM0) by FRP sheets (Mahini, 2005). As seen in Figure 1-(b), the relocation of the plastic hinge of the beam is shown (Mahini, 2005). Plastic hinge relocation using web-bonded FRPs has also been reported by Smith and Shrestha (2006).

(a) (b)

Figure 1. Failure mechanism of the joint (a) before (CSM0) and (b) after retrofitting by FRP sheets (RPSM2), Mahini, 2005).

3. DESCRIPTION OF SELECTED RC FRAME

The selected frame was an eight storey three bay OMRF as shown in Figure 2. The design dead and live loads are assumed to be 2,750 kg/m and 1,750 kg/m respectively. The compressive strength, f_c' and tensile strength, f_t of the concrete are taken as 27.46MPa and 3.668MPa, respectively. The elastic modulus of the concrete, E_c is taken as being 24.63GPa and the yield stress of steel reinforcement is taken as 412MPa. Design base shears are determined for a PGA of 0.3*g*. The weight of the system is taken as the dead load plus 20% of live load for the estimation of equivalent earthquake load based on the Iranian earthquake code (1999). Initial behaviour, *R* factor is assumed to be equal to 6 for all systems. The MRFs were designed based on *weak-beam strong-column* principle using ACI-95 (2005) Code and the steel bracing systems are designed using AISC-LRFD Code (1994). Dimensions and flexural reinforcements of the designed beam and column sections are shown in Figure 2. In this figure, ρ_t, ρ_s and ρ_s' are the total steel ratio of the column, and tensile steel ratio and compressive steel ratio of the beam respectively. All member and joint reinforcement has been designed to achieve the desirable strength and ductility (Maheri and Akbari, 2003).

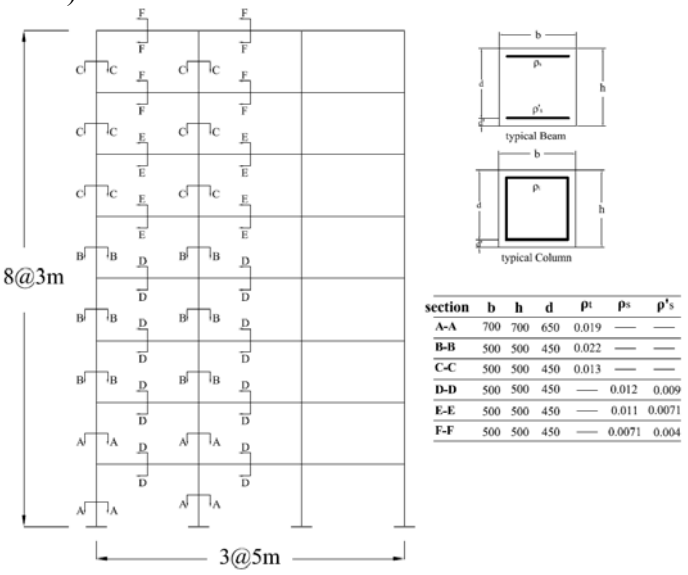

section	b	h	d	ρt	ρs	ρ's
A-A	700	700	650	0.019	—	—
B-B	500	500	450	0.022	—	—
C-C	500	500	450	0.013	—	—
D-D	500	500	450	—	0.012	0.009
E-E	500	500	450	—	0.011	0.0071
F-F	500	500	450	—	0.0071	0.004

Figure 2. Selected moment resisting frame (Maheri and Akbari, 2003).

4. NONLINEAR FINITE ELEMENT ANALYSIS OF RC JOINTS

In order to model the characteristics of concrete, ANSYS SOLID65 elements is used. This element is capable of simulating the cracking and crushing of the concrete.

To define a failure surface for concrete, two strength parameters, i.e., ultimate tensile and compressive strengths, are needed. During this study, it was found that when the crushing capability of the concrete is turned on, the finite element beam models fail prematurely. As a pure compression failure of concrete is unlikely, the crushing capability is turned off and therefore cracking of the concrete controlled the failure of the finite element models.

FEM input data for the SOLID65 element are Elastic modulus E_c, ultimate uniaxial compressive strength f_c', ultimate uniaxial tensile strength f_r, Poisson's ratio ν_c, for concrete, shear transfer coefficients β_t and β_c and the compressive uniaxial stress-strain relationship for concrete.

In this research, the ultimate uniaxial compressive strength f_c' and the elastic modulus of concrete E_c are obtained from standard compression tests on concrete cylinders. The ultimate uniaxial tensile strength f_r is calculated from $f_r = 0.6\sqrt{f_c'}$ for FE analysis of all specimens and the Poisson's ratio was taken to be 0.2. The concrete had a compressive strength around 27.46MPa and a modulus of elasticity around 24.63GPa. A modified version of the Hognestad's model for concrete typical stress-strain diagram is used (Mahini and Ronagh, 2010).

In addition, the best estimates of the behaviour are obtained if a shear transfer coefficient β_t of 0.3 is taken for open cracks. The shear transfer coefficient for closed cracks β_c is taken as 0.7, as recommended in the ANSYS online manual.

SOLID65 allows the presence of four different materials in the concrete element; one matrix material, and a maximum of three independent reinforcing materials that are assumed to be smeared throughout the element. Alternatively in this paper, in order to model the longitudinal reinforcement, a two-nodded link element, LINK8 has been used (ANSYS, 2005). The yield strength of the main steel reinforcements N12 and the stirrups R6.5 was approximately 500MPa and 382MPa respectively with a modulus of elasticity about 200 GPa. The Poisson's ratio ν_s of both reinforcements was about 0.3. For modelling the stress-strain properties of N12 steel bars, the stresses and strains of the steel at each straight line segments are required. For R6.5 stir-

rups, a bilinear model with a zero strain hardening modulus was used.

In addition, the FRP composites have been modelled using an eight-node three-dimensional multilayer solid element, SOLID45. CFRP sheeting possessed a tensile strength of about 3900MPa, a modulus of elasticity of 240GPa and an ultimate tensile elongation of 1.55%. ANSYS offers an anisotropic model called ANISO, which allows the introduction of the mechanical properties of FRPs in tension and compression in different directions (x, y, and z).

Ideally, the bond strength between the concrete and steel reinforcements should be considered. However, perfect bond between materials is usually assumed. To provide the perfect bond, the link element used for steel reinforcement is connected between the nodes of adjacent concrete solid elements, so that the two materials shared the same nodes. The same approach is employed for FRP composites assuming that a high strength epoxy is used to attach FRP sheets to the RC joint areas. Nodes of the FRP solid elements are connected to those of adjacent concrete solid elements in order to satisfy the perfect bond assumption.

Comparisons between the numerical predictions for the failure mechanisms of specimen and its experimental counterpart are shown in Figure 3. Good agreements between the results was observed, which indicates that the numerical analysis could be used as a practical tool for the analysis of repaired/retrofitted beam-column joints that encompass a web-bonded FRP system.

Mathematical modelling of typical exterior and interior joints is shown in Figure 4. Ten different exterior and interior models have been analysed by FE methods. In the following finite element modelling of the exterior and interior subassemblage are presented. The failure mechanism and moment-rotation relationship of the selected RC joints, retrofitted with CFRP web-bonded elements, (Mahini, 2005), was obtained using ANSYS (2005) software. Analytical models and the failure mechanism of an exterior and interior retrofitted joints are shown in Figures 5 and 6. The required FRP layers were designed based on the Mahini & Ronagh design charts (Mahini and Ronagh, 2006 and 2009).

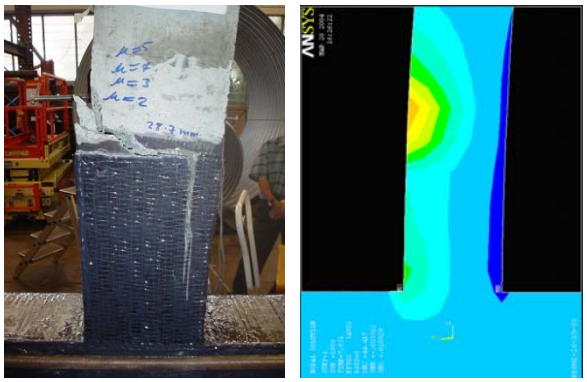

Figure 3. Experimental versus numerical failure mechanism of specimen RPSM2

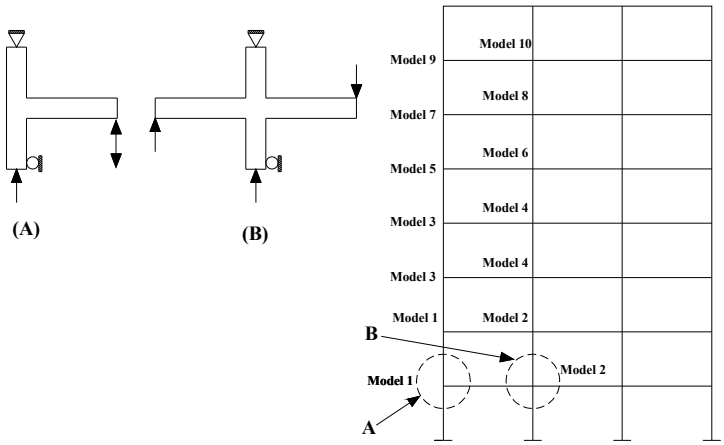

Figure 4. Analytical modelling of exterior and interior joints belongs to the selected frame under lateral loads.

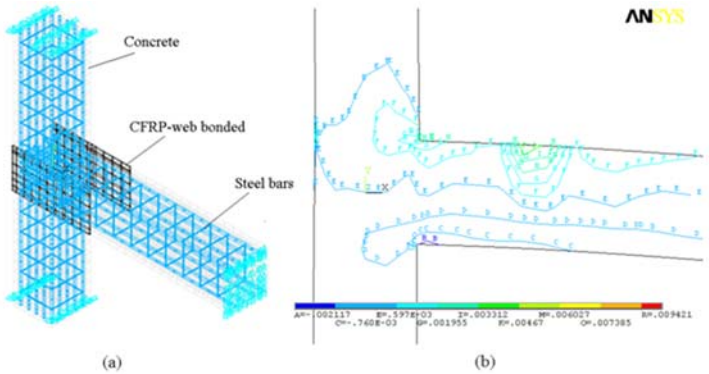

Figure 5. (a) Finite element model and (b) failure mechanism of an exterior retrofitted joint (Niroomandi et al., 2010).

Figure 7 shows the moment-rotation curves of an exterior beam-column joint at the third level of the selected frame. In Figure 7, K4 is the difference between the two curves. This relationship is also shown in Figures 8, 9 and 10 for all exterior and interior joints. This curve is different for the right and left side of the interior joint. The difference results from the different compressive and tensile reinforcements in the sections.

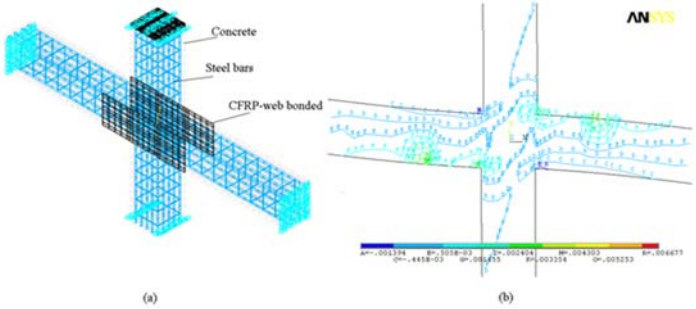

Figure 6. (a) Finite element model and (b) failure mechanism of an interior retrofitted joint (Niroomandi et al., 2010).

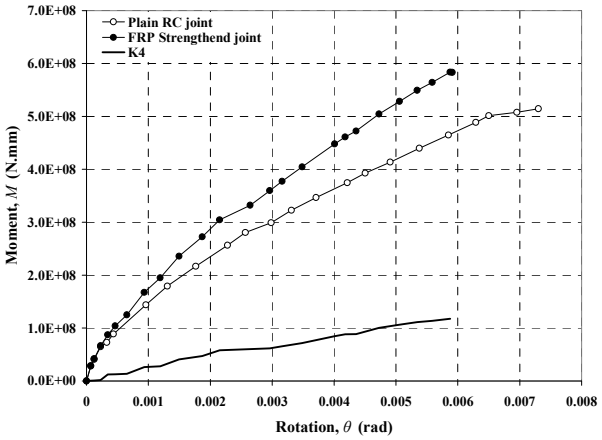

Figure 7. Moment-rotation curve of an exterior plain and FRP-strengthened joint.

In the FE analysis, in order to eliminate the effects of debonding failure of FRP sheets due to shear or normal stress concentrations at the end of the FRP, the maximum strain in FRP sheets was checked to ensure that it is less than the limiting quantities suggested by ACI 440.2 (2008). These limiting quantities are similar to the one proposed by Teng et al. (2003). According to this model, the effective strain in the FRP sheets is limited to the following expression in order to prevent the intermediate crack induced debonding mode of failure.

$$\varepsilon_{fd} = 0.41\sqrt{\frac{f_c'}{nE_f t_f}} \le 0.9\varepsilon_{fu} \qquad (1)$$

where, ε_{fd} is the maximum effective strain in the FRPs, f_c' is the concrete compressive strength, E_f and t_f are the elastic modulus and the thickness of the FRPs respectively and n is the number of FRP layers.

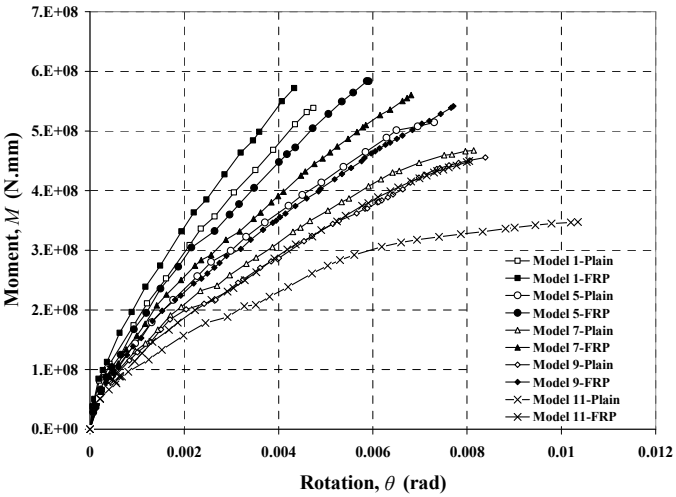

Figure 8. Moment-rotation curve for exterior plain and FRP-strengthened joints.

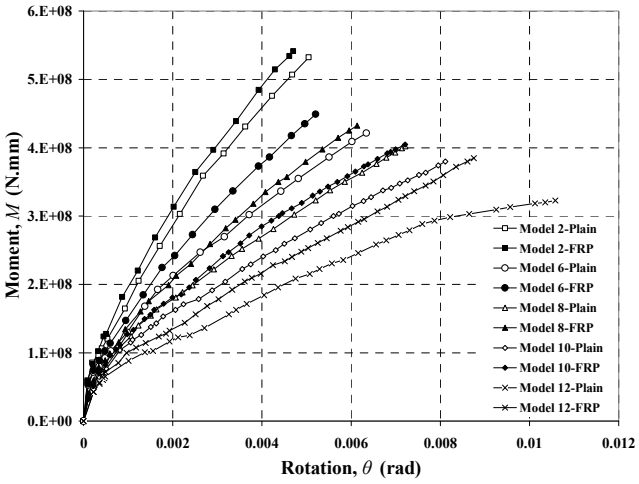

Figure 9. Moment-rotation curve for interior plain and FRP-strengthened joints on the right side.

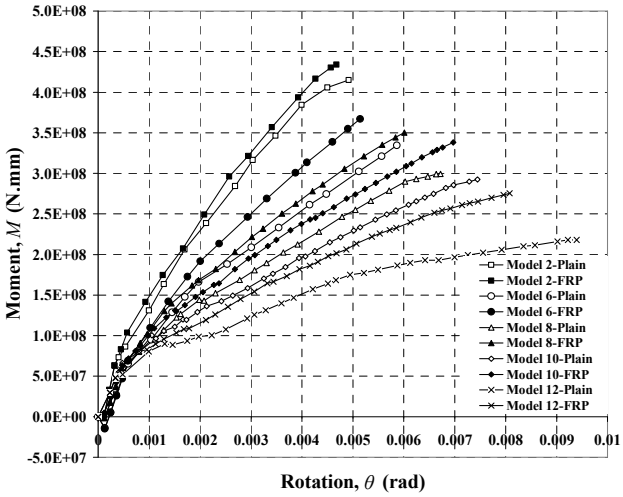

Figure 10. Moment-rotation curve for interior plain and FRP-strengthened joints on the left side.

5. PUSHOVER ANALYSIS OF THE SELECTED PLAIN AND RETROFITTED FRAMES

5.1 Plain Frame

Nonlinear pushover analysis of each system was carried out using the SAP 2000 (2006) program. For the inelastic pushover analysis of the frames, a constant gravity load equal to the total dead load plus 20% of the live load in accordance with the Iranian earthquake code (1999) was applied to each frame. An inverted triangular distribution over the height was used as the lateral load pattern. *P-Δ* effects were also considered in the analysis. Force-deformation criteria for the plastic hinges used in the pushover analysis was defined based on ATC-40 (1996) and FEMA356 (2000) regulations.

5.2. Retrofitted Frames

The analytical model of the retrofitted frame with FRP-web bonded system is shown in Figure 11. This frame has already been retrofitted by Maheri and Akbari (2003) using a steel-braced system. SAP 2000 non-linear link (NLLink), elements are used to model the FRP-retrofitted frames. These elements can simulate the equivalent additional beams stiffness provided by FRP web-bonded on the system. The element is assumed to be located at a distance of 500mm (because of FRP length) from the column face. This length was based on the Paulay & Priestley (1992) design approach for plastic hinge location. In Figure 11 each K is the additional rotational stiffness of each retrofitted beam that is modelled with non-linear link elements on the plain frame. The moment-rotation curve of plain and FRP retrofitted joints is taken from the FE analysis and the differences used as the rotational stiffness of retrofitted joints. The base shear versus roof displacement curves of plain and retrofitted (both steel-braced and FRP-retrofitted) frames are shown in Figure 12. In these curves, X-braced retrofitting systems examined by Maheri and Akbari (2003) were designed based on 50% and 100% of the lateral loading on the RC frames.

6. PERFORMANCE AND DAMAGE ASSESSMENT OF THE RETROFITTED FRAMES

6.1. Seismic performance assessment

The seismic performance level describes the limitation of the damage state of the frame structures. In fact, the intended post-earthquake condition of a building frame is a well-defined point on the scale measuring earthquake resistance loss. For this purpose, the capacity spectrum curve (S_a-S_d) of each system is determined and the performance level of each system is obtained from ATC-40 instructions, where S_d and S_a are the spectral displacement and acceleration respectively (see Figure 13). It also shows how the performance point (PP) of the FRP-retrofitted frame is obtained by ATC-40 instructions. In this figure, the base shear-roof displacement of the frame obtained from the pushover analysis has drawn incorporated into the S_a-S_d curves from the Iranian Code for Earthquake Design of Building 2800, (1999). Based on the Iranian Code, 5% damped response spectrum with earthquake acceleration base design of 25% of the gravity acceleration value was used to obtain the performance point of each frame. In this investigation, the exact solution of the ATC-40 document was used in order to calculate the PP of all systems. Figure 14 shows the Acceleration Displacement Response Spectra (ADRS) curve and the performance level of all frames.

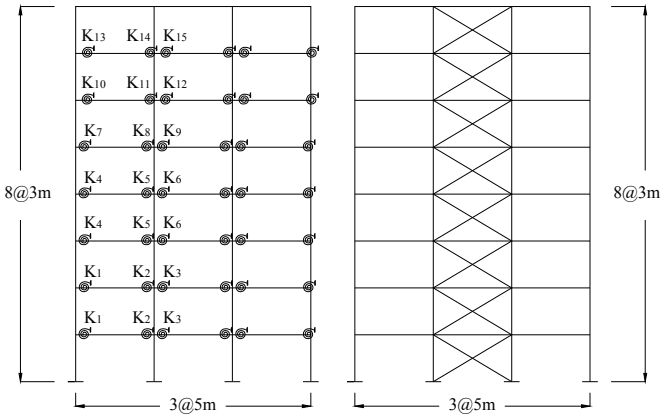

Figure 11. Analytical modelling of the (a) CFRP web-bonded (current study) and (b) steel-braced frame (Maheri and Akbari, 2003).

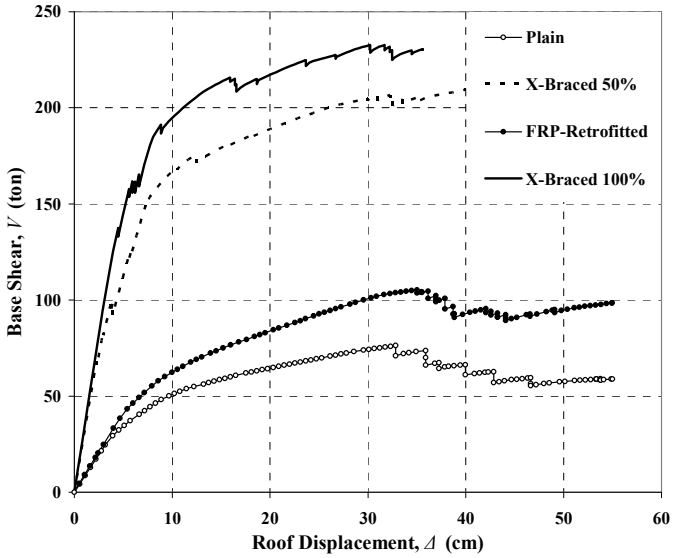

Figure 12. Base shear-roof displacement curves of all frames.

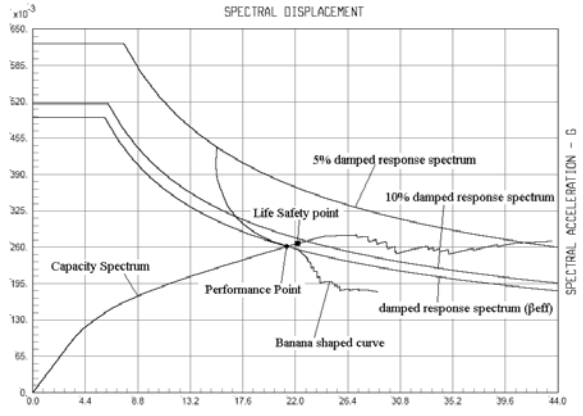

Figure 13. ADRS curve for estimating performance level of FRP Retrofitted frame (based on ATC40) (Niroomandi et al., 2010).

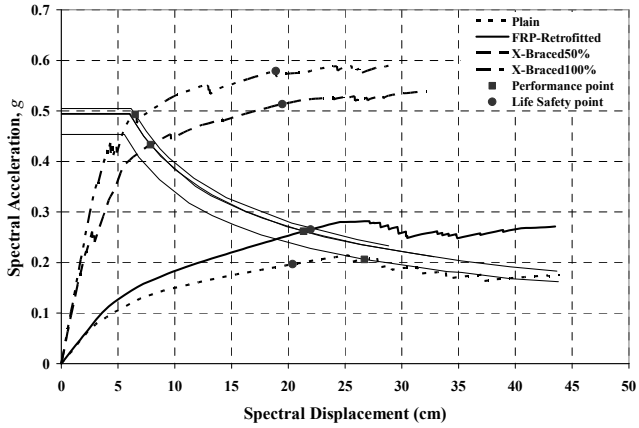

Figure 14. ADRS curve and the performance level of each frame.

According to Figure 14 and Table 1 in the original frame, the performance point has a spectral displacement of 26.7cm. The performance point of the FRP retrofitted frame also has a spectral displacement of 21.24cm. Such a reduction in the spectral displacement for the FRP retrofitted frame indicates that the inelastic lateral load resistance has been enhanced through web-bonded FRP retrofitting. Also, the shift in the performance point of the frame due to joint retrofitting has resulted in an increase in the spectral acceleration value from 0.206g to 0.262g. This indicates that there has been an increase in the seismic load capacity for the FRP retrofitted frame. However, the reduction in the spectral displacement due to X-bracing of the frame is far more profound than that in the joint FRP retrofitted case; being around 7.9 and 6.5 for the 50% and 100% brace load share cases respectively. This shows a substantial increase in the inelastic lateral capacity of the braced frames. The large differences between the lateral load resistances of the steel-braced frames compared with the joint FRP retrofitted frame are expected, as the strong bracing systems were designed especially to increase the stiffness and the lateral strength capacity of the RC frame. However the web-bonded FRP retrofitting of the frame at joints is designed to increase joint rotation capacities, relocate the plastic hinges and, in general, improve the seismic performance of the frame.

Figure 15 shows the plastic hinge distribution of each frame at the target displacement. As shown the plastic hinge distribution of the FRP-retrofitted frame is improved in comparison to the plain frame. Also based on this presentation and the ATC-40 regulations, performance point coordinates of all systems are calculated as shown in Table 1. As it can be seen, the FRP-retrofitted frame satisfies the life safety (LS) level.

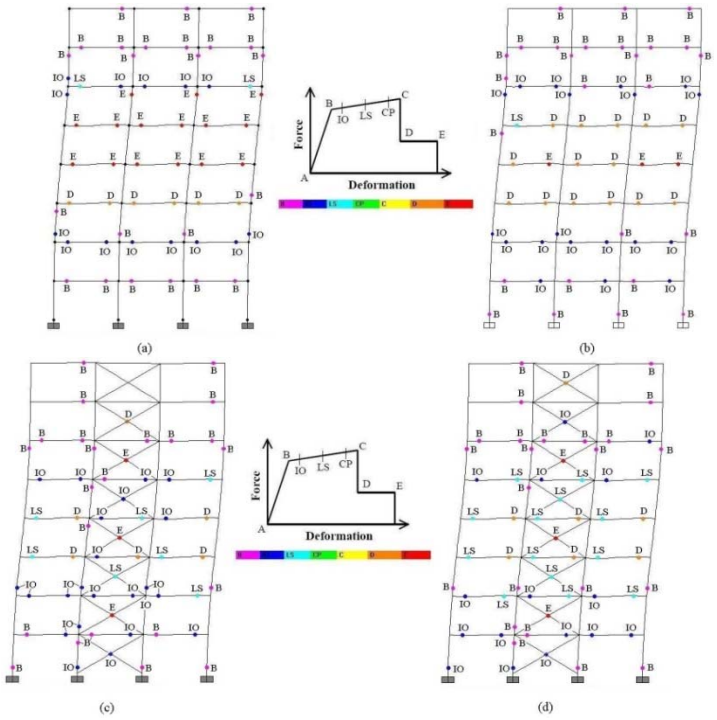

Figure 15. Plastic hinge distribution of the frames: (a) Plain; (b) FRP-retrofitted; (c) X-Braced 100%; (d) X-Braced 50% (Niroomandi et al., 2010).

6.2. Ductility

Displacement ductility is an important parameter in assessing the inelastic seismic performance of RC frames. The displacement ductility ratio μ_m, is calculated using Eq. (2).

$$\mu_m = \frac{\Delta_{\max}}{\Delta_y} \tag{2}$$

Table 1. Performance level of each system

Frame	PP						LS			
	S_d (cm)	S_a (×g)	Δ(cm)	V(ton)	Adjusted Δ(cm)	Adjusted V(ton)	S_d	S_a	Δ(cm)	V(ton)
Plain	26.7	0.206	35	70.8	46.7	56.75	20.392	0.197	25.8	70.84
X-Braced 50	7.88	0.433	10	167	13.4	175	19.464	0.5135	26.5	200
X-Braced 100	6.516	0.493	8.75	187.5	11.67	200	18.917	0.5788	24.4	228
FRP Retrofitted	21.353	0.262	27.5	96.8	36.7	100	21.972	0.2655	29.5	100

Table 2. Ductility ratio and Global Damage Index (Dc) of all systems, * (Maheri and Akbari, 2003), ** Current study

Frame	μ_m	D_c @ PP	Adjusted D_c @ PP	Damage Degree@ PP	D_c @ LS	Damage Degree@ LS
Plain	2.27*	0.67	0.8	Severe	0.43	Moderate*
Xbraced-50%	2.84*	0.39	0.5	Moderate	0.72	Severe
Xbraced-100%	2.7*	0.22	0.38	Moderate	0.66	Severe
FRP Retrofitted	2.94**	0.51	0.62	Moderate	0.53	Moderate

*Performance point (PP) is located after life safety (LS) which is not satisfactory

Where, Δ_{max} and Δ_y, are the ultimate displacement and the yield displacement of the base shear versus roof displacement curve, respectively.

A number of performance parameters may govern the capacity of a structure. In order to carry out an inelastic pushover analysis, one or a number of these parameters should be considered for the determination of the displacement limit state (Δ_{max}). For the regular medium-rise, ductile (*weak beam-strong column*) buildings considered in this study, the global drift (maximum roof displacement) is used as a common failure criterion. In evaluation of the displacement ductility μ, the ultimate capacity of each frame was assumed when the global drift reached 1.5% of the system height. This criterion is based on the NEHRP recommendations (1997) for RC moment resisting frames. The idealized force-displacement curve obtained based on the FEMA-356 method for the FRP-retrofitted frame is shown in Figure 16. In this figure, V_y and Δ_y, are yield strength and yield displacement respectively. Δ_t and V_t are the target displacement and the corresponding base shear respectively. The displacement ductility of all systems is tabulated in Table 2. The ductility ratio of FRP-retrofitted frame is improved by 30% whereas the X-braced's ductility increased by 25%.

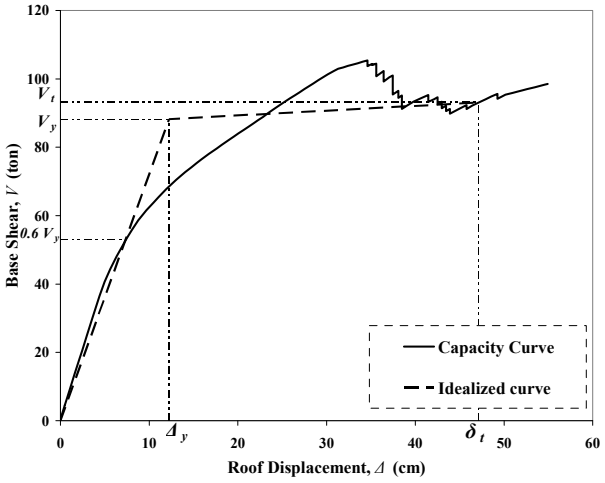

Figure 16. Capacity curve and Idealized curve of FRP retrofitted frame (based on FEMA356).

6.3 Damage assessment based on capacity curve

6.3.1 Background

The state of damage of the whole structure may be represented by an index. This damage index can be used as an indicator to describe the reserve capacity of existing structures and the state of the lateral load-carrying capacity of the building.

Based on the fundamental parameters, various local and global damage indices have been proposed to evaluate RC structures. Structural ductility, storey drift, element and connection rotation, energy dissipation, and fatigue of the structure are the parameters that have been considered for damage assessment (Haoxiang et al., 2013).

Research on the global damage indices is ongoing because the integral damage assessment should be accurate and consider the local damage of the elements (i.e. beams and columns). However, most of the presented global damage indices are limited due to their limited convergence for considering the cumulative damage. In addition, a significant amount of research has shown that the capacity spectrum method can simplify be used for assessment of the structural performance. Therefore damage indices can be obtained from pushover analysis and capacity curve based on the PBD strategy (Dipasquale and Cakmak, 1989). Although the capacity spectrum method (pushover method) has major simplifications, such as the multi-degree of freedom system being transformed into a single-degree of freedom system, it can be an alternative to time-consuming nonlinear time-history analyses. However, the accumulated dissipative effect is not sufficiently considered in the evaluation of regular structures.

Some local damage indices have been proposed to calculate damage of each component of the building. A global damage index for the structure may be integrated from the component damage indices using a weighting procedure. These damage indices have been formulated using response parameters of the structure that are obtained from structural analysis. Several techniques and approaches for damage analysis of structures can be used. These are pushover analysis, nonlinear time history analysis, and vulnerability analysis. The typical response based damage indices include inter-story drift, ductility ratio, slope ratio, flexural damage ratio, maximum drift, final softening index, low cycle fatigue and Park-Ang index (1994). The inter-story drift and maximum drift damage indices are expressed by displacement or deformation.

One of the most acceptable damage indexes is the Park-Ang damage index in which both ductility and cumulative hysteretic energy demand are combined [10, 26]:

$$D_{PA} = \frac{\delta_m}{\delta_u} + \frac{\beta}{\delta_u F_y}\int dE_h \qquad (3)$$

where δ_m is the maximum experienced deformation, F_y is the yield strength of the element, δ_u is the ultimate deformation of the element, $\int dE_h$ is the hysteretic energy absorbed by the element and β is the model constant parameter, which for nominal strength deterioration is equal to 0.1.

Typically, a perfect damage index is within a scale of 0 to 1, where zero represents undamaged state and 1 represents the building collapse. The Park-Ang damage index is over 1 and in some cases nearly close to 2. This damage index is not directly suitable for nonlinear static pushover analysis method because the cumulative damage is not occurred in this analysis (Haoxiang et al., 2013).

A global stiffness damage index of the RC frames was presented by Ghobarah et al. (1999) based on pushover analysis as follows:

$$D_k = 1 + \frac{k_F}{k_I} \qquad (4)$$

where k_I is the initial slope of the base shear-top floor deflection curve obtained from the pushover analysis of the frame before subjecting it to the earthquake ground motion and k_F is the initial slope of the curve after withstanding the earthquake action. This damage index has a range from zero to one.

Although this global stiffness damage index can be computed based on pushover analysis only, without carrying out other dynamic analysis, it is not accurate for moderate damage or the collapse stage where the index may exceed 1 and the cumulative effect is not taken into account.

A global damage index is proposed by combining the stiffness damage index and Park-Ang damage index. Referring to Eq. (3), a similar stiffness damage index can be expressed as:

$$D_c = 1 + \frac{k_c}{k_o} \qquad (5)$$

where k_0 is the initial stiffness at the elastic stage and k_c is the current stiffness.

Based on Eq. (5), the corresponding force F_c, can be obtained from current displacement u_c and the damage index as follows. $F_c = k_o(1 - D_c)u_c$ (6)

The typical skeleton curve or capacity curve of the RC frame can be presented with an equivalence multiple linear as shown Figure 17, and according to Eq. (6), the current force between the i^{th} point and the $i+1^{th}$ point can be expressed as;

$$F_c = k_o u_1 + k_1(u_2 - u_1) + k_2(u_3 - u_2) + \ldots + k_{n-1}(u_n - u_{n-1}) + k_n(u_c - u_n) \quad (7)$$

where $k_i = (F_{i+1} - F_i)/(u_{i+1} - u_i)$.

Finally, a general damage index for capacity curve can be obtained by substituting to Eq. (7) in Eq. (6) as shown:

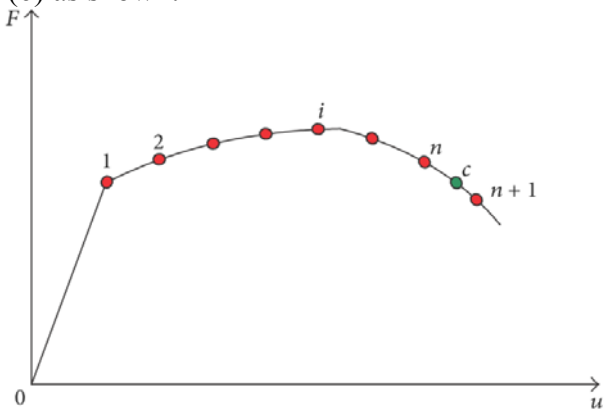

Figure 17: Multiple linear force-deformation curve (SAP2000, 2006).

6.3.2 Damage-Index Adjustment Considering Hysteretic Energy

During strong ground motion, the performance capacity of structures is reduced due to the cumulative damage caused by cyclic loads. However, as mentioned above, the pushover analysis does not embody the cumulative damage sufficiently and therefore, a modified coefficient is essential in obtaining reliable estimates.

For this purpose, an equivalent (reduced) ductility factor has been proposed by Fajfar (1994). The parameter γ, which is a function of maximum displacement, dissipated hysteretic energy and the natural frequency of the structural system is introduced as follows:

$$\gamma = \frac{\sqrt{E_h / m}}{\omega \delta_m} = \frac{1}{\mu_u}\sqrt{\frac{E_h}{m}} \quad (9)$$

where E_h is the total hysteretic energy, $\mu_u = \delta_u/\delta_y$ in which δ_y is the yield displacement, and μ_u is the normal ductility, and δ_m is the monotonic displacement or current displacement. The monotonic ductility factor μ_m, can be obtained from $\mu_m = \delta_m/\delta_y$. The transformation can be then obtained from:

$$D_c = 1 - \frac{\sum_{i=0}^{n-1} k_i (u_{i+1} - u_i) k_n (u_c - u_n)}{k_o u_c} \quad (8)$$

This general global damage index which has a range of 0 to 1 is calculated based on base shear-top floor deflection curve obtained from only one push-over analysis. In addition, it is suitable to obtain the damage index of any displacement such as the PP and LS points.

$$\frac{E_h}{F_y \delta_y} = \gamma^2 \mu_m^2 \quad (10)$$

where F_y is the yield strength of the system that can be estimated as $F_y = m\omega^2\delta_y$ in which m is the mass, ω is the natural frequency of the system.

Substituting to Eq. (9) into Eq. (3), the Park-Ang damage index is rewritten as:

$$D_{PA} = (1 + \beta\gamma^2 \mu_u)\frac{\mu_u}{\mu_m} \quad (11)$$

Thus, the relationship between displacement ductility factor on cumulative damage of the building under seismic action and the displacement ductility factor subjected to monotonic load is as follows:

$$\frac{\mu_u}{\mu_m} = \frac{D_{PA}}{(1 + \beta\gamma^2 \mu_u)} \quad (12)$$

For normal structure, the ratio μ_u/μ_m ranges from 0.65 to 0.85 (Haoxiang et al., 2013).

By applying Eq. (12) to Eq. (8) the damage index for considering dissipated hysteretic energy can be computed. For the performance point (PP), where the shear-roof displacement of the frame and the capacity spectrum curve intersect, the corresponding displacement ductility is viewed as μ_u. . However, the damage in pushover analysis is related to the monotonic ductility μ_m. Hence, the displacement on the performance point can be amplified according to Eq. (12) in order to represent the actual damage.

6.3.3 Damage assessment

The shear-roof displacement of the frame and the capacity spectrum curve of all plain and retrofitted frames is represented with equivalence multiple linear as shown in Figure 18. In this figure, the global damage indexes are calculated based on Eq. (8) at the performance point, the adjusted point according to Eq. (12) and the life safety point (see Table 1). The global damage indices of all frames are shown in Table 2.

Damage assessment is established according to the damage degree description in Table 3 (Haoxiang et al., 2013) and the damage degree and the limit values as illustrated in Figure 19.

According to Table 2, the plain frame is in severe damage at the adjusted performance point whereas; both the steel-braced frames and the FRP-retrofitted frame are at moderate degrees of damage. This is exactly matched with the ductility factor improvements of the retrofitted frames compared with the plain frame. On the other hand, at life safety, the FRP-retrofitted frame indicates a moderate degree of damage compared with the steel braced frame which experiences severe damage at LC. However, the moderate degree of damage of the plain frame is not acceptable as the LC point is reached before the PP, which is not satisfactory based on the ATC-40 standard.

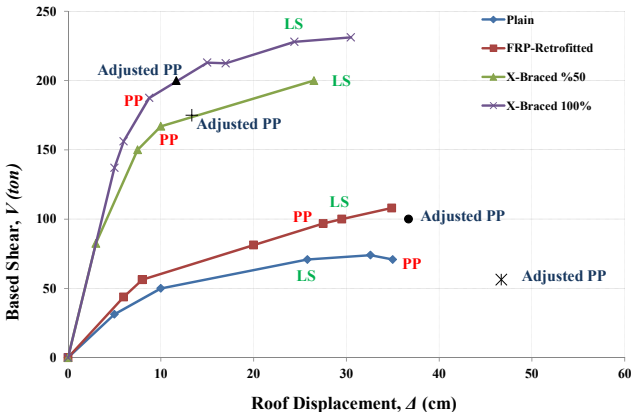

Figure 18. Multiple linear force-deformation curve for plain and retrofitted frames

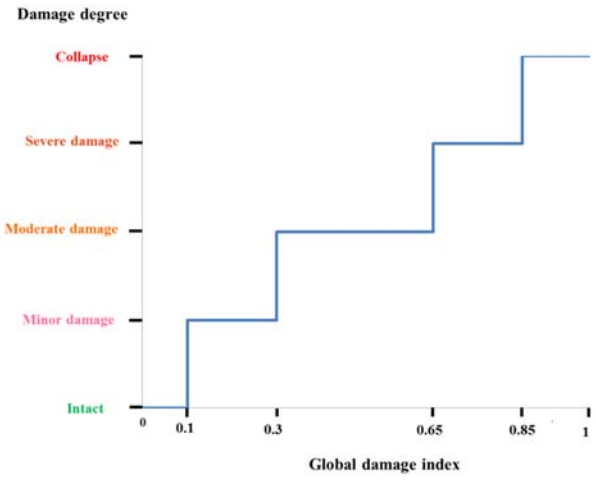

Figure 19. Damage degrees and the limit value for different damage indices.

In Figure 20 this demonstrated trend is noticeable. Both retrofitting systems have reduced the degree of damage of the plain frames at the performance point (PP). This improvement was more clearly indicated with respect to the life safety (LS) demand where the FRP-retrofitted frame has the lowest degree of damage among the retrofitted frames. The plain frame has been rejected in terms of performance based assessment criteria.

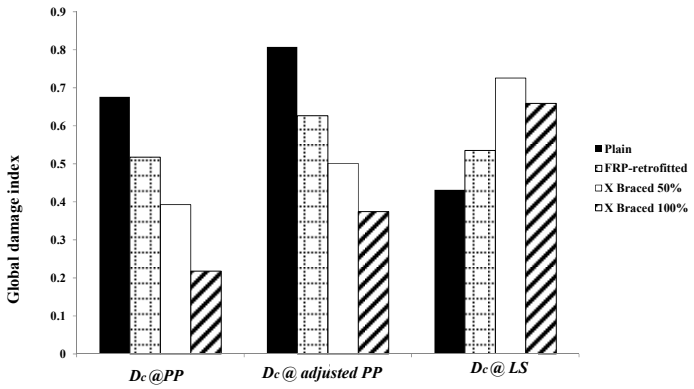

Figure 20. Global damage index of the plain and retrofitted frames at PP, the adjusted PP and the LS.

7. CONCLUSIONS

Conventional retrofitting systems in earthquake-resisting frames have limitations. For example, steel bracings systems considered in this paper for verification of the new proposed web-bonded FRP retrofitting system is able to dissipate considerable energy by yielding under tension and buckle, without much energy dissipation in compression. Because of this, an eight storey frame that was previously strengthened with a steel bracing system, was selected and was retrofitted with bonding FRP on the web of its beams at the joints. In order to estimate the flexural stiffness of the FRP retrofitting system, nonlinear FE analysis was adopted. A systematic evaluation of each system including the ductility ratio and performance level evaluation was made using nonlinear static pushover analysis. The additional flexural stiffness of the FRP joints is added to the frame using nonlinear link on the beam end of each exterior and interior joint.

Based on the results, it is concluded that the performance level of FRP retrofitted RC frame for LS is satisfactory. In addition, the displacement ductility factor of FRP-retrofitted RC frame is up to 30.9 and 3.5 percent higher than the 100% X-braced and 50% X-braced frames respectively.

The damage index determination is necessary to assess the degree of damage of existing retrofitted reinforced concrete structures subjected to seismic action. For this purpose, a global damage index is presented based on multiple linear force-deformation curves obtained from pushover analysis. A modified coefficient was adopted based on a consideration of the cyclic load and hysteresis energy.

It is evident that the weak stories are in failure (*strong beam-weak column* was more obvious) in the plain frame resulting in collapse in a strong earthquake. Therefore, maintenance and retrofitting should be carried out for moment resisting frames in earthquake prone regions. The damage of FRP-retrofitted frame is moderate at both PP and LS. The damage of both steel-braced frames is severe at LS, but the capacity and the performance requirements are met at PP.

Consequently the web-bonded CFRP system (when carefully designed) could upgrade the performance of the existing OMRFs in a ductile manner. It can also change the damage degree of the frame from severe to moderate.

8. REFERENCES

ACI 440.2R-08, "ACI Committee 440-02. Guide for the design and construction of externally bonded FRP system for strengthening concrete structures", MCP 2005. ACI. Michigan (USA); 2008.

ACI Committee 318, "Building code requirements for reinforced concrete (ACI 318-95) and commentary (ACI 318R-95)", American Concrete Institute, Detroit, Michigan, 1989.

American Society of Civil Engineering (ASCE), "Prestandard and Commentary for the Seismic Rehabilitation of Buildings", prepared for the Federal Emergency Management Agency, FEMA 356, 2000.

ANSYS. ANSYS Manual set., ANSYS,Inc., Canonsburg, PA 15317, USA, 2005.

ATC, "Seismic Evaluation and Retrofit of Concrete Buildings", ATC-40, Applied Technology Council, Redwood City, 1996.

Balsamo A, Colombo A, Manfredi G, Negro P, Prota A. Seismic Behavior of a Full Scale RC Frame Repaired using CFRP Laminates. *Engineering Structures*, 2005;27:769-780.

Dipasquale, E., and Cakmak, A. S., "On the relation between local and global damage indices," Technical Report NCEER-89-0034, State University of New York at Buffalo, 1989.

Fajfar, P., "Consistent inelastic design spectra: hysteretic and input energy,"*Earthquake Engineering & Structural Dynamics*, vol. 23, no. 3, pp. 523–537, 1994.

Federal Emergency Management Agency (FEMA). "NEHRP provisions for the seismic rehabilitation of buildings", Rep FEMA 273 and 274, Washington DC, 1997.

Ghobarah, A., Abou-Elfath, H. and Biddah, A. "Response based damage assessment of structures," *Earthquake Engineering & Structural Dynamics*, vol. 28, no. 1, pp. 29–104, 1999.

Hadigheh, S. A., Mahini, S.S. and Maheri, M.R., "Seismic Behaviour of FRP-Retrofitted Reinforced Concrete Frames", *Journal of Earthquake Engineering*, 2014, 18:1171–1197, 2014.

Haoxiang H., Maolin C. and Yongwei L., "Earthquake Damage Assessment for RC Structures Based on Fuzzy Sets", Hindawi Publishing Corporation, Mathematical Problems in Engineering, Volume, 2013; Article ID 25486525:1-11. http://dx.doi.org/10.1155/2013/254865

Maheri MR, Akbari R. Seismic behavior factor, R, for steel X-braced and knee-braced RC buildings, Engineering Structures 2003; 25:1505-1513.

Mahini, S.S., "*Rehabilitation of Exterior RC Beam-Column Joints using CFRP Sheets",* PhD thesis submitted to the Division of Civil Engineering of the University of Queensland, Australia, 2005.

Mahini, S. S. and Ronagh, H. R., "Strength and ductility of FRP web-bonded RC beams for the assessment of retrofitted beam–column joints", *Composite Structures*, 2010, 92(6), 1325-32.

Mahini, S. S. and Ronagh, H. R., "Web-bonded FRPs for relocation of plastic hinges away from the column face in exterior RC joints", *Composite Structures*, 2011, 93, 2460–2472.

Mahini S.S., Ronagh H.R. "Computer Model for Repaired RC Beams Using Web-Bonded FRP Sheets", Proceeding of the Second International Conference on Concrete Repair, Concrete Solutions, June 27-29, St-Malo, France, 2006, 115-122.

Mahini, S. S., and Ronagh, H. R. "Numerical modelling of FRP strengthened RC beam-column joints", *Structural Engineering & Mechanics*, 2009, 32(5), 649-65.

Manual of Steel Construction, Load and Resistance Factor Design, LRFD. 2nd ed. American Institute of Steel Construction, Chicago. III, 1994.

Naeim F., "Real-Time Damage Detection and Performance Evaluation for Buildings, in Earthquakes and Health Monitoring of Civil Structures", Springer Environmental Science and Engineering 2013, pp 167-196.

Niroomandi, A., Maheri, A., Maheri, M. R. and Mahini, S. S., "Seismic performance of ordinary RC frames retrofitted at joints by FRP sheets", *Engineering Structures*, 2010, 32(8), 2326-36.

Park, Y. J., Ang, A. H. S., and Wen, Y. K.,"Seismic damage analysis and damage limiting design of R.C. buildings," Structural Research Serial Report UILU-ENG-84-2007, University of Illinois at Urbana-Champaign, Urbana, Ill, USA, 1984.

Paulay T, Priestley MJN. "Seismic Design of Reinforced Concrete and Masonry Buildings", John Wiley & Sons, INC, 1992.

Parvin A, Granata P., "Investigation on the Effects of Fiber Composites at Concrete Joints", *Journal of Composites part B*, 2000; 31:499-509.

SAP2000 Non-linear version 10.1.0. "Analysis Reference Manual", Computers and Structures Inc., Berkeley, Calif, 2006.

Smith ST, Shrestha R., "A Review of FRP Strengthened RC Beam Column Connections", *Proceeding of the Third International Conference on FRP Composites in Civil Engineering (CICE 2006)*, 13-15 December-Miami, Florida, USA, 2006, 661-664.

Teng JG, Smith ST, Yao J, Chen JF. "Intermediate crack induced debonding in RC beams and slabs". Constr Build Mater 2003; 17(6–7):447–64.

Iranian code of practice for seismic resistance design of buildings, standard no.2800 2nd edition. 1999.